Proc. 6th Asia-Pacific Conf. on Shock and Impact Loads on Structures, Perth, pp. 445–456 (2005).

SCALED SHOCK MEASUREMENTS USING MICRO-SCALE FIBRE OPTIC PRESSURE TRANSDUCERS

Aleksey V. Pichugin, Andrew Tyas*,
Department of Civil and Structural Engineering,
University of Sheffield, S6 3RQ, UK

William N. MacPherson, Stuart Watson, and James S. Barton
School of Engineering and Physical Sciences,
Heriot-Watt University, Edinburgh, EH14 4AS, UK

Abstract

Conventional piezo-electric blast pressure transducers suffer from a number of problems, including sensitivity to radio-frequency (r.f.) noise and acceleration. An alternative fibre-optic transducer has recently been developed which offers a promising alternative. This form of transducer comprises a single fibre-optic cable which terminates in a small cavity, capped with a diaphragm. Laser light is directed along the cable and reflects from the diaphragm. Displacement of the diaphragm due to an external pressure results in a phase shift in the wavelength of the reflected light which can be recorded and calibrated against pressure. These transducers are essentially insensitive to acceleration and r.f. interference, and in addition, are extremely small (diaphragm diameters are below 100μm) providing excellent spatial resolution of pressure readings and offering the possibility of an almost non-intrusive sensor, which is of great benefit in small-scale model testing of blast effects. This paper describes a series of small scale experimental trials using these transducers for the measurement of the interaction of blast waves with rectangular structures. The sensors are used to capture the overpressure and impulse acting on barriers; their small size allows careful measurement of effects such as clearing around the boundaries of the barriers. Their performance relative to conventional piezo-electric transducers is discussed, and the results compared to empirical data from ConWep.

Keywords: fibre-optic transducers, hemispherical blast waves, overpressure, parameter scaling.

* Corresponding author. Tel./fax.: +44 114 222 5735/5700, email: a.tyas@sheffield.ac.uk

1. Introduction

When looking into diffraction of blast waves around obstacles an experimentalist is faced with the necessity of accurate measurement of shock parameters near obstacle surfaces. Knowledge of time history of shock overpressure can be very useful for understanding flow around the obstacle, however it is notoriously difficult to measure precisely. An ideal pressure transducer must be insensitive to r.f. interference and thermal disturbances, present in the vicinity of a chemical explosion. It must also have low acceleration sensitivity to reduce amount of the acoustic interference produced, for example, by ground shocks or structural resonances. Finally, such transducer must exhibit low (sub microsecond) risetimes, necessary to adequately reproduce structure of shock waves. The last requirement is not only temporal but also spatial, because most practically observed shocks are not plane and would not be able to load large sensing elements uniformly, which results in increased perceived risetimes for the recorded signal. This difficulty is particularly relevant, although not restricted, to side-on measurements of blast wave overpressure.

Thus, there is a substantial interest to new methods for accurate sensing of rapidly varying pressure. One possible design for such transducers has been described in [1], in which sensor body with a flexible diaphragm was fixed at the end of an optical fibre. Movement of the diaphragm caused by the change in an external pressure alters the distance between two reflective surfaces: cleaved end of the optical fibre and the diaphragm itself. This enables very accurate interferometric measurements of the diaphragm deflection, which for small deflections varies linearly with pressure. Low weight of the diaphragm ensures low acceleration cross-sensitivity. Spatial dimensions of the sensor are only limited by the diameter of the optical fibre. Original design of these sensors comprised 3μm thick copper diaphragm glued to zirconia body, 2.5mm in diameter. Diameter of the sensing area, 125μm, matched the diameter of the optical fibre and guaranteed linear response for pressures up to 10bar (1MPa) with the resonance frequency around 500kHz. These gauges were demonstrated to successfully perform in the blast environment and survived repeated testing, see [2].

In order to further reduce sensor dimensions and improve the overall sensor performance new generation of sensors has recently been designed. By using techniques typical for the modern semiconductor industry, new sensor bodies were made on a silicon wafer. This technology is widely available and, if mass produced, similar fibre optic gauges may in the future become an inexpensive, possibly disposable alternative to traditional sensors. In particular, most of the fibre optic gauges used in our trials had 2μm composite silicon dioxide/silicon nitride diaphragms, with diameters between 50μm and 100μm and resonance frequencies in the megahertz range, which linearly respond to pressures of up to 8bars. Brief overview of the sensor construction and chosen interrogation scheme is provided in Appendix.

Data is currently being gathered on blast wave diffraction around simple structures, which could be relevant to a civil engineer. The purpose of our project is to improve our understanding of scaling of experimental conditions involving blast waves interacting with rigid structures, with particular emphasis on small scale and near-field testing. Even for well-studied laws for scaling of spherical and hemispherical blasts, there is an understanding that commonly available empirical data on blast wave parameters, see e.g. tables in [3], figures in [4] or software “ConWep” [5], based on tests by the American military, have limitations on both range of scaled distances and size of the charges. Nevertheless, these limits are not specified explicitly and usually have to be re-estimated for every particular experimental environment. The situation is even more complicated if chosen explosive is different from TNT, because commonly used constant TNT-equivalency factors should actually be functions of the scaled distance, see [6].

A series of 19 trials that we describe here was aimed at evaluating performance of new generation of fibre-optical sensors as well as investigate the applicability of the available scaling data in the near-field of the small scale explosion. Square (2×2m) test arena was designed to faithfully reproduce conditions of a hemispherical blast. Hemispherical explosive charges were placed at the centre of the arena and initiated near the surface by a detonator inserted through the special aperture. Overpressure data were collected from front and top surfaces of two rectangular test structures. One of the test structures was instrumented with two piezo-electrical gauges, whereas another — with array of six fibre optic gauges as well as two piezo-electrical gauges for comparison and control. Surface of the test arena remote from the test structures was instrumented with an extra side-on piezo-electrical gauge to identify features present in the blast wave before interaction with structures begins.

The principal results of this paper include arrival time and positive reflected impulse data recorded at the front and top faces of the test structures. Peak reflected overpressures were also analysed but appeared to be less informative. Considerable attention was paid to the phenomenon of second shock, which is generated in the negative phase of the main shock during explosion of any sufficiently strong (hemi-) spherical charge, see e.g. numerical or experimental work [7,8]. While overpressure and positive impulse of the second shock in an open air appears to be relatively insignificant, diffracted blast wave may exhibit second shock compatible with the first. This, for example, happens at the top face of a rectangular obstacle.

On the whole, low response times and high spatial resolution of the used fibre optic sensors enabled quite detailed interpretation of the obtained data, for example, identification of multiple shocks travelling across the face of a structure if the Mach stem was formed. Release waves are also more evident on the overpressure traces from fibre optic sensors.

2. Test environment

Hemispherical blast is, perhaps, the simplest configuration of blast wave relevant for civil engineering. Many practically important situations of blast loading of structures may be well approximated by this configuration, even though practical charges are very rarely ideal hemispheres placed at the surface and initiated at the centre. However, modelling of hemispherical blast waves presents some difficulties. Firstly, the appropriate hemispherical charges would inevitably act as contact charges and therefore crater the surface, thus invalidating the assumption of surface uniformity. Secondly, the initiation of the charge exactly at the surface level poses additional difficulties. An experimental setup was developed to address these problems and enable repeated loading of various simple structures with hemispherical blast waves.

2.1. Test arena

A rigid surface is simulated in our tests by square 2×2m sheet of 12mm thick steel, supported at approximately 1m above the floor by a frame made of 100×100mm 10mm thick steel box section, see Figure 1. All four legs at the corners of the test arena were bolted to the floor to ensure stability of the structure. Extra support was provided by hydraulic jacks that were used to prop the surface sheet at the middle of the longest spans. The arena was placed into an explosion room with the distance to the nearest wall over 1m and about 2m between ceiling and arena surface. This ensured that the diffraction phenomena were not obscured by spurious reflections.

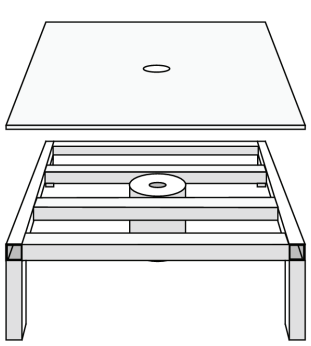
(a)

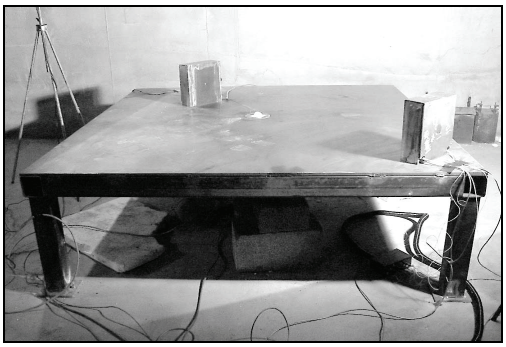
(b)

Figure 1. (a) Drawing of the frame that supports the test arena. (b) The arena before a trial with two test structures. A hemispherical explosive charge is placed at the centre.

Since the centre of the test arena had to withstand repeated contact explosions, special supporting column was prepared, see Figure 2. In order to address the inevitable cratering of the arena in the vicinity of a charge, a round hole, 154mm in diameter, was cut at the centre of a surface sheet. Explosive charges were initiated on top of the sacrificial anvils, 150mm discs of 20mm thick mild steel, which were inserted into the hole and lied on top of the main anvil, 600mm diameter disc made of 80mm thick steel and supported by a piece of steel tube. As the thickness of sacrificial anvils (20mm) was greater than the thickness of the surface sheet (12mm) an extra 8mm padding ring was placed onto main anvil. A deliberate impedance mismatch between

sacrificial anvils and the main anvil slightly decreased the amount of arena vibration. Since sacrificial anvils are not fixed to the rest of the structure there was a risk of catapulting it when the arena rebounds. This was prevented by adding a thin layer of viscous decoupler between the anvils, which also somewhat reduced high-frequency table vibration. Charge initiation was performed by a detonator inserted through the 7mm aperture at the centre of sacrificial anvil. Detonation cable was fed through the opening at the side of the supporting tube and into the cable aperture at the centre of main anvil.

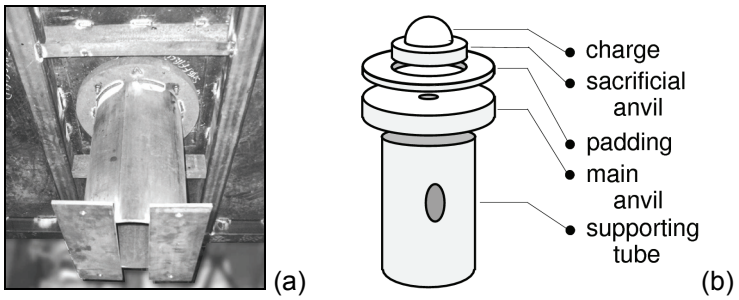

Figure 2. (a) Photograph of a column, which supports the test arena under the charge. (b) Illustrative diagram with the principal components of the column.

Main anvil was welded onto the supporting tube, which was bolted to the floor. The surface steel sheet, padding ring and main anvil were not welded, only bolted together to simplify disassembly. This was done because the test arena will later be used for trials with up to half a kilogram of high explosive and the current supporting column is not robust enough to withstand repeated testing of this kind.

2.2. Test structures

Rectangular test structures had to be spot welded onto the surface and, consequently, were designed for ease of instrumentation. Piezo-electric and fibre optic gauges were placed flush with the front and top faces of the removable front part (a) of a test structure, see Figure 3. Most of the front part is made of single 270mm long 260mm wide piece of channel section, 13mm thick at the sides and 7mm thick at the front. Top is capped with a sheet of 10mm steel, welded onto channel section. Special care was taken to ensure that corners of the test structures were perfectly rectangular. Rear part (b) of every test structure was instrumented with no sensors and therefore was easy to spot weld onto the test arena. During a trial front part (a) was bolted to the rear part (b) and padded at the front with a polymer strip, which substantially reduced the amount of cantilever vibrations natural to such structure. It is worth noting that stiffening ribs shown at the rear part (b) of test structure were also introduced to increase natural frequency and reduce amplitude of the cantilever vibrations.

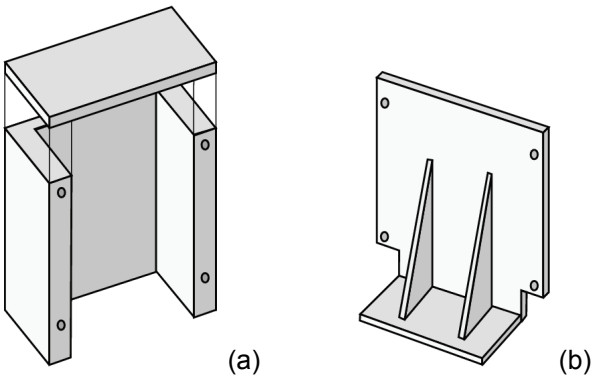

Figure 3. Drawing of an opened test structure. Rear part (b) is spot welded onto the surface of test arena, whereas front part (a) is bolted to it for ease of instrumentation.

Overall dimensions of the prepared test structures were 260×270×100mm. In order to minimise the interaction between flows diffracted around each structure they were placed as far apart as

possible, along diagonals of the test arena. Two structures were used in every trial at distinct distances from the charge, so that range of covered scaled distances could be extended further.

2.3. Sensor configuration

Three of the piezo-electric gauges used in our trials were Kulite HKM-375 fabricated in special blast resistant casing with sensing area about $9\pi \cdot mm^2$. Since we felt that relatively large sensing area of these sensors may conceal details of shocks diffracted around the test structures, two smaller Kulite XCQ-80 gauges were also employed. These sensors are made in the form of 2mm diameter steel cylinders with effective sensing area under $\pi \cdot mm^2$. Both types of gauges were previously tested with approximately plane shocks and demonstrated risetimes on the microsecond scale.

Our experimental equipment enabled simultaneous acquisition of up to six fibre optic gauges. In order to enable interoperability between the piezo-electric and fibre optic sensors, all of the latter were mounted into Kulite style cases, see Figure 4. Square 1×1mm sensor bodies composed of silicon can be seen at the centre of passive sensing area on both provided photographs. Effective sensing area for all employed fibre optic sensors never exceeded $0.0025\pi \cdot mm^2$; resonance frequencies of these gauges lie above 500kHz.

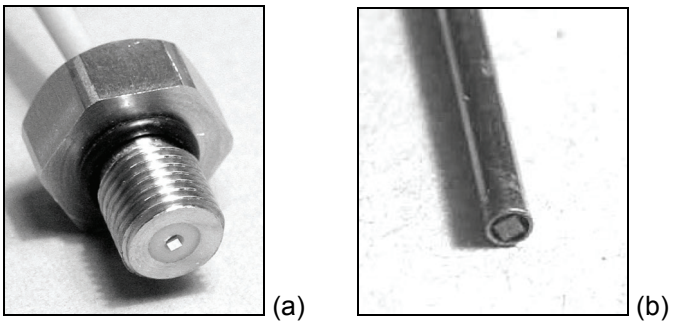
(a) (b)

Figure 4. Photographs of the employed fibre optic sensor mountings: (a) Kulite HKM-375 style mounting; (b) Kulite XCQ-80 style mounting.

Two test structures were used throughout the described series of trials. Test structure A, see Figure 5(a), was fixed at one of the test arena diagonals, 654mm from the arena centre. Since structure A was situated relatively close to the blast source, it was instrumented with piezo-electric sensors only: gauges #1 and #6 were mounted at the centre of front and top faces, respectively. Test structure B, see Figure 5(b), was placed at the opposite end of the same diagonal, 1010mm from the centre, thus ensuring that the minimum distance between any of the structures and the other structure, room walls or ceiling exceeded 1.5m.

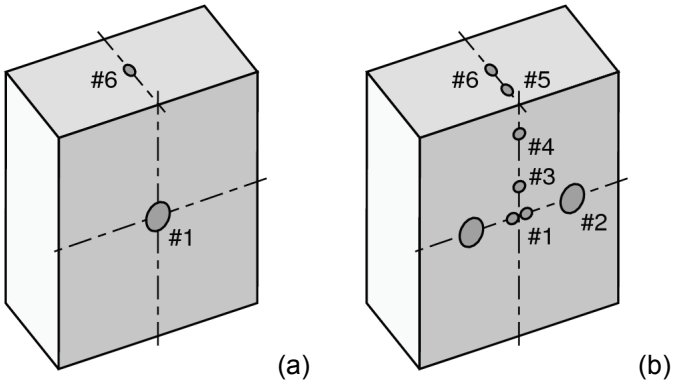

(a) (b)

Figure 5. Sensor positions for the test structures A and B. Bigger circles correspond to gauges in Kulite HKM-375 style mounting, smaller circles — to Kulite XCQ-80 style mountings.

The fibre optic sensors were mounted into array arranged to track propagation of blast wave from the centre of front face (position #1) to the centre of top face (position #6). In order to collect sensor comparison data, readings of the fibre-optic sensors in positions #1 and #2 were

duplicated by the symmetrically placed Kulite gauges. An additional piezo-electric gauge was mounted directly at the free diagonal of the test arena surface. This side-on gauge, placed 783mm away from the arena centre, was used to gather control data free from any diffraction phenomena.

2.4. Experimental procedure

Hemispherical charges weighing between 30g and 70g were formed from PE4, an inexpensive and safe to handle plasticized high explosive, widely used by the engineering community. Lower limit of the charge size was selected to reduce influence of a detonator, which in our case ("Demolition L2A1") is equivalent to approximately 1.5g of high explosive. Upper charge size limit was selected to guarantee that the test arena suffers no permanent damage.

Overpressure data was recorded using variety of acquisition systems, including scopes Gould 630 and LeCroy 9304, as well as data logging units by Microlink and NI. Data acquisition systems were trigged by a breaking wire circuit, with the breaking wire coiled around top end of the detonator inserted into the charge. Ideally, we would prefer to initiate the explosive directly at the surface of the test arena, however, blast safety rules require the detonator to be inserted into the charge. For the series of trials described in this paper typical effective height of the explosion centre is situated 3–5mm above the test arena surface.

3. Experimental results

Instead of a relatively inefficient procedure of moving the test structures to change Hopkinson ("cube root") scaled distance ($m/kg^{1/3}$), we opted to vary size of the explosive charge itself. This has substantially improved turn-around time of the experiments and extended range of available scaled distances. But before discussing the results of our trials it is worth mentioning possible limitations of the implemented experimental procedure.

Essentially, the assumption that we make by varying the charge size instead of the distance to the charge is: Hopkinson scaling is valid. If no correlation with other experimental data is observed the implication is that for the considered data the Hopkinson scaling is not valid. This situation is often observed in the vicinity of an explosive charge, which motivates the notion of blast near-field, see e.g. [9]. Indeed, it is known from the numerical modelling of blast waves produced by pressurised spheres (one of better approximations of the chemical explosion) that the Hopkinson scaling is only valid when blast wave travelled sufficiently far from the source, see [10]. This phenomenon is sometimes referred to as the "late stage equivalence" of blast waves. Scaling of such blasts in the near field requires more complex scaling law incorporating additional parameters of the charge.

Another and more serious consideration is possible influence of energy losses during the explosion. One of the possible loss mechanisms is dispersion of thin layer of high explosive adjacent to the free surface, which would explain phenomenon of critical charge diameters. Since this effect would be less pronounced for large charges, we may expect better correlation with the available scaling data for bigger charges. However, at the scale of our testing this effect may be partially compensated by extra energy released by the detonator.

3.1. Hemispherical blasts and Mach stem formation

Configuration of a hemispherical blast wave is an idealised configuration and it is difficult to reproduce it in an experiment exactly. It is, for example, difficult to reproduce perfectly rigid impenetrable surface for the blast wave or to initiate the charge in a perfectly hemispherical fashion. Because of the sensor array instrumented at one of the test structures we were able to verify satisfaction of the necessary experimental conditions. The expectation is that for accurately reproduced hemispherical blast wave our gauges at the test structure B should register single shock travelling from the sensor position #1 towards the sensor position #6, see Figure 6(a). We may also expect to see release waves produced when the shock is diffracted around the top edge and travelling back towards ground. Example of a successful test is provided in Figure 6(b), where shock is travelling upwards as is expected and small release wave spike is visible on the trace from the sensor in topmost front face position #4.

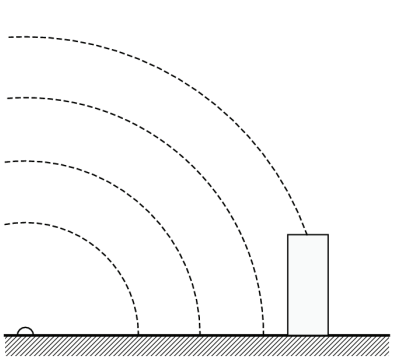
(a)

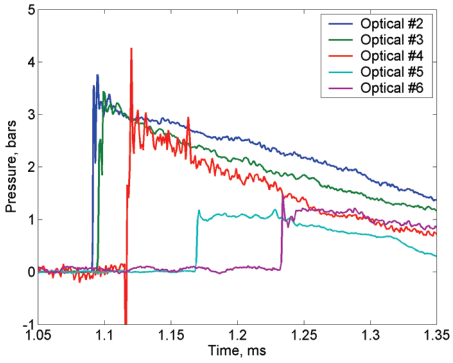

(b)

Figure 6. (a) Idealised diagram illustrating propagation of a hemispherical blast; (b) Blast wave arrivals from a trial number 8 with 40g charge.

In our setup, the most significant departure from the requirements of a hemispherical blast is a non-zero height of the charge initiation centre. The situation is further complicated by directional effects of the used detonators. An expected result of this setup limitation is formation of a Mach stem, an irregular reflection occurring when a blast wave hits the surface near grazing incidence. Incoming and reflected shocks are then joined in the "Y" shape and travel together along the surface, so that a side-on measurement would register a single shock, although strengthened by the reflection. We compared arrival times recorded by our side-on gauge with the predictions of ConWep to check whether Mach stem was formed, see data in Table 1.

Charge size, g	30	40	50	60	70
Arrival time, ms	0.737	0.664	0.603	0.558	0.520
(s.d. 0.022ms)	(0.753)	(0.695)	(0.652)	(0.618)	(0.591)

Table 1. Averaged arrival times from the side-on gauge versus corresponding predictions from ConWep (in brackets). S.d. stands for the standard deviation.

The observed arrival times are substantially lower that the predictions of ConWep. This may indicate stronger shocks, which is to be expected if the Mach stem was formed. Interestingly, most practically available hemispherical blast data were obtained by explosive charges placed near the ground level. The assumption is that if charge is initiated sufficiently close to the ground, trajectory of triple point of the Mach "Y" lies high above the test structures and resulting shock is very similar to one where no Mach stem was produced. However, even with special efforts to initiate explosive charges very close to the arena surface we recorded substantial number of blast waves featuring diffraction of Mach "Y" around the test structure. The expected diffraction phenomena are sketched in Figure 7(a).

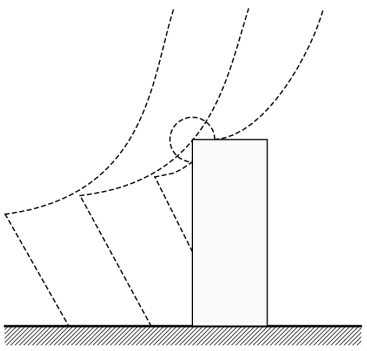
(a)

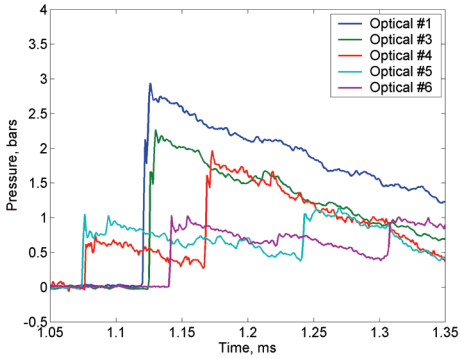

(b)

Figure 7. (a) Schematic diagram illustrating propagation of a blast wave involving the Mach stem; (b) Blast wave arrivals from a trial number 19 with 40g charge.

An example of this situation is provided in Figure 7(b). An incoming spherical part of the shock first hit the structure near the corner and was almost simultaneously registered at sensors positions #4 and #5. Approximately 0.05ms later obliquely reflected Mach stem reached positions #1 and #2. The reflected spherical shock travelling down the front face of the test structure and

the Mach stem travelling up met somewhere below position #1, because traces in positions #1 and #3 feature no well pronounced double shocks.

Traces obtained in trials of this kind are of no use for analysing scaling of blast waves, because they feature up to four separate shocks joined in a positive phase of a blast. Peak pressure measurements are not possible in this situation, whereas registered positive impulses are substantially higher then would be expected for a single reflected shock. Because of this difficulty we had to discard over one third of the collected data, see Table 2. The number of trials with multiple shocks seems to increase when the charge size is increased, which can be explained by lower position of the triple point trajectory at small scaled distances.

Charge size	30g	40g	50g	60g	70g
Number of trials (with no multiple shocks)	4 (3)	5 (3)	4 (2)	4 (2)	2 (1)

Table 2. Information on number of trials with no multiple shocks.

It is worth noting that arrival time data still could be and was gathered from these traces. The discarded data only included peak pressures and positive impulses.

3.2. Arrival times, peak pressures and positive impulses

In this section we discuss blast wave parameters registered at the centre of front face of test structure B. All of the data is averaged and compiled into Table 1, along with maximum standard deviations and corresponding predictions by ConWep.

Charge size, g	30	40	50	60	70
Arrival time, ms (max s.d. 0.037 ms)	1.187 (1.191)	1.112 (1.106)	1.001 (1.042)	0.959 (0.991)	0.903 (0.949)
Peak reflected pressure, bars (max s.d. 0.60 bars)	2.70 (3.22)	3.57 (4.21)	4.07 (5.11)	5.16 (6.03)	7.10 (6.96)
Positive reflected impulse, bars-ms (max s.d. 0.146 bars-ms)	0.684 (0.746)	0.761 (0.918)	0.881 (1.08)	1.11 (1.23)	1.28 (1.38)

Table 3. Averaged data from the centre of front face of test structure B, provided together with the corresponding ConWep predictions (in brackets).

Arrival time data is known to be relatively easy to measure accurately and good correlation between observed and predicted data for smaller charges in Table 3 is extra evidence for that. The correlation is less impressive for bigger charges, which indicates that at the small scale ConWep is applicable for arrival time predictions when the scaled distances are over 3 m/kg$^{1/3}$. In order to verify this statement side-on arrival time data of Table 1 were plotted together with the data from Table 3, see Figure 8. The trend in side-on arrival times is clearly similar and also suggests identifying 3m/kg$^{1/3}$ as approximate minimum applicable scaled distance.

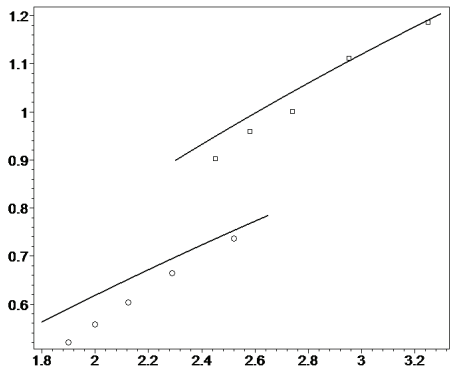

Figure 8. Arrival time (ms) versus scaled distance (m/kg$^{1/3}$) at the face of test structure B (boxes) and at the side-on gauge (circles), shown along with ConWep predictions (solid lines).

Similar trends may be observed in the data for peak pressures and positive reflected impulses. Any correlation is lost when charge size is increased, because it corresponds to lower scaled distances from the charge. Data in the Table 3 demonstrates that "Loads on structures" component of ConWep consistently overestimates both peak reflected pressures and positive reflected impulses for all scaled distances under 3.2m/kg$^{1/3}$.

3.3. Second shock

In all of the data collected during our trials we observed the phenomenon of second shock. This shock is travelling in the negative phase of blast wave and never catches up with the main shock, see Figure 9(a). Second shock produces relatively small overpressures, approximately 20% of the main shock or less; positive impulse of the second shock is hard to compute for the lack of well-defined boundary between positive and negative phases, however it may be estimated to be 15% of the positive impulse of the main shock or less. The rule of thumb for our experimental environment is that the arrival time of the second shock is roughly double the arrival time of the main shock. This indicates that second shock cannot be produced by a reflection since the test arena has no reflecting surfaces that are sufficiently close. It is also not a diffraction phenomenon because it is registered by the side-on gauge.

Existence of the second shock is predicted by numerical and analytic models of the explosion of a pressurised sphere, which is also a good approximation to a chemical explosion, see [7]. It cannot be obtained in a shock tube. At the current stage we decided against publishing arrival time and approximate impulse data for the second shock because our experimental setup can substantially affect its formation. Specifically, the second shock that we are seeing is a back travelling shock produced during the blast expansion and reflected at the origin. It would therefore be affected by the moving sacrificial anvil, which is also substantially deformed by the time the second shock gets to the arena centre. We intend to modify the test setup to circumvent this difficulty in a forthcoming series of trials.

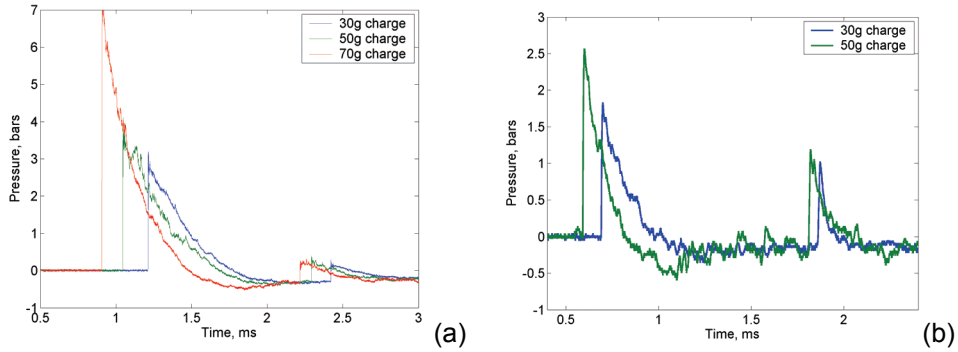

Figure 9. Typical examples of second shock at (a) centre of the front face of test structure B or (b) centre of the top face of test structure A.

When second shock travels through open areas or simply reflected from the obstacles it remains relatively insignificant, however, the gauges mounted at the top of our test structures regularly registered diffracted second shocks which possessed positive impulses up to 50% of the main shock and overpressures of the same order of magnitude; couple of relevant examples are presented in Figure 9(b).

3.4. Performance of fibre optic sensors

Fibre optic sensors performed quite reliably throughout the testing. Associated interrogation gear has all been connectorised and can be prepared to an experiment and operated by a non-specialist. Although peak pressure limit of about 1MPa precluded use of fibre optic gauges in both test structures, their advantages clearly compensated for the inconvenience. First and foremost, low weight of the diaphragm resulted in very low acceleration sensitivity, enabling substantially more accurate data capture and interpretation, e.g. compare Figure 9 (a) and (b).

It seems that improved temporal resolution of the fibre optic sensor does not provide any substantial improvements to the quality of captured data. Observed risetimes are probably lower

than those of piezo-electric gauges, but exact figures are difficult to pinpoint because of the substantial variations in the diffracted wave fields around the test structures between various trials. Low risetimes sometimes produced by the piezo-electric gauges are usually caused by aliasing effects associated with the time that transient shock has to travel to fully load the sensing area. The main improvement to the quality of data is, therefore, due to extremely small sensing area of the fibre optic sensors, which enables easy distinguishing between various small transient shocks travelling around the obstacle.

4. Conclusion

A new optical pressure transducer has been successfully used to measure blast wave parameters from small scale explosive charges. These transducers have the advantages of very small size, insensitivity to electrical noise and relatively low sensitivity to acceleration. Initial results obtained from tests using these gauges indicate that empirical scaling relations give reasonable approximations even when charge sizes are very small. The signals recorded by these gauges also highlight other features of the blast waves, notably the presence of a strong second shock which is predicted by theoretical analyses. These gauges will be used in a forthcoming series of larger explosive trials, and the results reported at a later date.

Acknowledgement

This research has been supported by the UK Engineering & Physical Sciences Research Council and Dstl Fort Halstead through the MoD Joint Grants Scheme.

Appendix

Principle of operation of the used fibre optic sensors as well as corresponding interrogation scheme have been reported elsewhere, see [11]. This brief appendix provides only very basic description of the sensor design. An extrinsic Fabry-Perot interferometer was formed between the cleaved end of an optical fibre and a reflective diaphragm, exposed to the measured pressure. The diaphragm was formed at the end of a micro-machined sensor body that holds the fibre in a recessed hole. The resulting hermetically sealed 30–120μm cavity, see Figure 1, was filled with air at an ambient pressure. Resulting cavity (and effective diaphragm) diameters ranged between 50μm and 100μm, offering control of sensitivity versus maximum operating pressure.

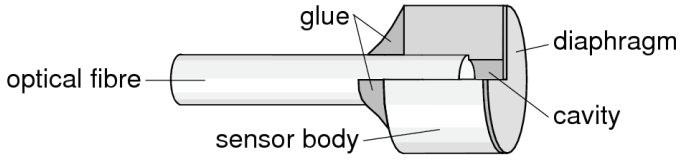

Figure 1. Schematic diagram of the fibre optic sensor with quarter of the body taken out.

Sensor bodies were produced on a 3-inch 380μm thick silicon wafers by using deep silicon etching. The diaphragms were thermally grown on separate wafers and transferred to the main wafer by a bonding technique. This wafer was subsequently diced into individual 1×1mm sensor bodies. The necessary reflectivity of the inner diaphragm surface was achieved by coating it with 10nm to 100nm thermally evaporated aluminium layer. Sensor assembly was finalised under a microscope by an operator guiding a cleaved fibre end into the entry hole. When fully inserted, the fibre was glued to the body using epoxy.

In order to interrogate the sensors, light from three wavelength stabilised 10mW laser diode sources at 1532nm, 1547nm and 1563nm was coupled into a 1550nm single-mode optical fibre. Low reflectivities of the fibre/air interface and inner diaphragm surface resulted in a nearly sinusoidal response of the returned intensity versus external pressure. For small deflections, i.e. when the diaphragm acts as a membrane, the observed variation of optical phase against pressure was approximately linear. The use of three interrogation wavelengths overdetermined

the optical phase data, so that the system was insensitive to common mode intensity noise and possible variations in the visibility of interference.

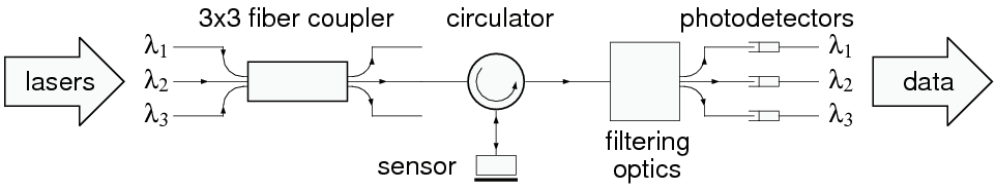

Figure 2. All-optical interrogation scheme, shown for one of the sensors.

The diagram in Figure 2 illustrates one channel of three available in each of our interrogation units. Chosen sensor interrogation scheme is all-optical, in particular, the wavelength filtering is implemented using fibre Bragg gratings. We were running two interrogation units simultaneously, receiving data from six optical sensors.

References

[1] MacPherson, W. N., Kilpatrick, J. M., Barton, J. S., & Jones, J. D. C. (1999) Miniature fiber optic pressure sensor for turbomachinery applications, *Review of Scientific Instruments,* **70**(3), pp. 1868–1874.

[2] MacPherson, W. N., Gander, M. J., Barton, J. S., Jones, J. D. C., Owen, C. L., Watson, A. J., & Allen, R. M. (2000) Blast-pressure measurement with a high-bandwidth fibre optic pressure sensor, *Measurement Science and Technology,* **11**, pp. 95–102.

[3] Kinney, G. F., & Graham, K. J. (1985) *Explosive Shocks in Air,* New York: Springer-Verlag.

[4] Smith, P. D., & Hetherington, J. G. (1994) *Blast and Ballistic Loading of Structures,* Oxford: Butterworth Heinemann.

[5] Conventional Weapons Effects ("ConWep", 1991), is a computer programme, based on the content of technical manual TM 5-855-1 (1986) *Fundamentals of protective design for conventional weapons,* Structural Laboratory, Waterways Experimental Station, for the Department of the Army, US Army Corps of Engineers.

[6] Wharton, R. K., Formby, S. A., & Merrifield, R. (2000) Airblast TNT equivalence for a range of commercial blasting explosives, *Journal of Hazardous Materials,* **A79**, pp. 31–39.

[7] Brode, H. L. (1959) Blast wave from a spherical charge, *The Physics of Fluids,* **2**(2), pp. 217–229.

[8] Boyer, D. W. (1960) An experimental study of the explosion generated by a pressurised sphere, *Journal of Fluid Mechanics,* **9**, pp. 401–429.

[9] Ismail, M. M., & Murray, S. G. (1993) Study of the Blast Wave Parameters from Small Scale Explosions, *Propellants, Explosives, Pyrotechnics,* **18**, pp. 11–17.

[10] Chou, P. C., & Huang, S. L. (1969) Late-stage equivalence in spherical blasts as calculated by the method of characteristics, *Journal of Applied Physics,* **40**, pp. 752–759.

[11] Gander, M. J., MacPherson, W. N., Barton, J. S., Reuben, R. L., Jones, J. D. C., Stevens, R., Chana, K. S., Anderson, S. J., & Jones, T. V. (2003) Embedded micromachined fiber-optic Fabry-Perot pressure sensors in aerodynamics applications, *IEEE Sensors Journal,* **3**, pp. 102–107.